J. Fluid Mech. (1990), *vol.* 221, *pp.* 289–310
Printed in Great Britain

Time-dependent helical waves in rotating pipe flow

By MICHAEL J. LANDMAN†
Courant Institute of Mathematical Sciences, New York University, 251 Mercer Street, New York, NY 10012 USA

(Received 9 June 1989 and in revised form 11 May 1990)

The Navier–Stokes equations for flow in a rotating circular pipe are solved numerically, subject to imposing helical symmetry on the velocity field $\boldsymbol{v} = \boldsymbol{v}(r, \theta+\alpha z, t)$. The helical symmetry is exploited by writing the equations of motion in helical variables, reducing the problem to two dimensions. A limited study of the pipe flow is made in the parameter space of the wavenumber α, and the axial and azimuthal Reynolds numbers. The steadily rotating waves previously studied by Toplosky & Akylas (1988), which arise from the linear instability of the basic steady flow, are found to undergo a series of bifurcations, through periodic to aperiodic time dependence. The relevance of these results to the mechanism of laminar–turbulent transition in a stationary pipe is discussed.

1. Introduction

Flow through a circular pipe provides a number of interesting and challenging problems in the study of fluid stability. Known as Hagen–Poiseuille flow when the pipe is stationary, the flow of an incompressible viscous fluid forced through a pipe has been known to be sensitive to instabilities since the studies of Reynolds (1883). Yet the nature of the transition from a laminar axisymmetric and parabolic velocity profile to one of localized 'puffs' of more complex (turbulent) motion when the axial Reynolds number of the flow is increased (proportional to the pressure gradient driving the flow) remains essentially a mystery. This is chiefly because there is no linear instability mechanism involved as the Reynolds number is increased. If the pipe is rotated about its axis, however, the initial process of transition is better understood, as it follows a linear instability scenario leading to wave-like structures, found experimentally by Nagib, Lavan & Fejer (1971).

The purpose of the work reported here is to study the secondary instability processes of rotating Poiseuille flow to a class of perturbations with helical symmetry. Although helically symmetric flows are strictly only two-dimensional, their study may in turn shed more light on the fully three-dimensional instability of Hagen–Poiseuille flow. In this introduction we briefly summarize what is known about Hagen–Poiseuille flow, and then move onto the more recent work concerning rotating pipe flow.

In experiments conducted by Leite (1959), pipe flow was found to be stable up to at least axial Reynolds number $R_D = 13000$, provided inlet velocity fluctuations were kept controlled ($R_D = \bar{U}D/\eta$ where $\bar{U}$ is mean cross-sectional velocity, D is the pipe diameter, and η is the kinematic viscosity of the fluid). A number of theoretical

† Present address: BHP Melbourne Research Laboratories, PO Box 264, Clayton, Vic 3168, Australia.

and numerical studies on linear stability also lead to the conclusion that the flow is stable to all infinitesimal disturbances at any axial Reynolds number. For instance, the stability of the flow to infinitesimal axisymmetric and non-axisymmetric perturbations is comprehensively studied numerically by Salwen & Grosch (1972) and Garg & Rouleau (1972). Therefore, the nature of instability in Hagen–Poiseuille flow appears to be subcritical (i.e. a threshold amplitude is required to trigger instability), a fact recognized by Reynolds in his seminal experiments.

In order to investigate the stability of Hagen–Poiseuille flow to non-axisymmetric disturbances experimentally, Fox, Lessen & Bhat (1968) periodically perturbed the flow with a small vibrating spring inside the pipe, thereby locally setting up a helical disturbance. By monitoring the disturbance amplitude downstream of the spring as a function of the mass flux and the electromagnetic forcing frequency, they were able to map out a stability diagram in the (R_D, α)-plane, where α is the wavenumber of the disturbance in the axial (downstream) direction. Their results indicate that fully developed laminar flow is stable to helical disturbances of fixed amplitude (2% of the centreline velocity) for Reynolds numbers less than 2150, and that there is a 'nose' of instability, in that only a finite band of wavenumbers α are unstable for a fixed R_D. These results are a consequence of a nonlinear instability mechanism which is still not understood.

In contrast to the linear stability of stationary pipe flow, it is curious that if the pipe is rotated about its axis with a relatively small (but finite) angular velocity, the basic flow, which is now a combination of the parabolic Poiseuille flow and solid body rotation, is destabilized. This linear instability was first established by Pedley (1969) in the limit of large rotation Ω, small axial wavenumber α, and finite axial Reynolds number $R_z (R_z = U_0 r_0/\eta$ where U_0 is the centreline velocity and r_0 is the pipe radius), by studying normal mode perturbations to the parabolic base flow of the form

$$\boldsymbol{v} = \boldsymbol{v}_0(r) + \epsilon \boldsymbol{v}_1(r)\, \mathrm{e}^{\mathrm{i}(n\theta+\alpha z)+\sigma t}. \tag{1}$$

R_z is the Reynolds number that has been traditionally used in theoretical studies, and $R_z = R_D$ for the undisturbed flow (in which $U_0 = 2\bar{U}$).

Mackrodt (1976) studied the stability of rotating pipe flow numerically, and found that the flow could be unstable with small pipe rotation for a sufficiently large axial Reynolds number in a given range. In this slow rotation regime the unstable waves also have $\alpha \ll 1$, as do Pedley's fast rotation modes. For all values of the wavenumber and azimuthal and axial Reynolds numbers, the instability is found to occur only if the corresponding eigenfunction has a screw-sense (in space) which is the same as that of the underlying swirling laminar flow ($\alpha\Omega < 0$ for $n > 0$); however, waves can be found that rotate (in time) in either sense, as viewed in the laboratory frame (Cotton & Salwen 1981). Cotton & Salwen perform an extensive study of the stability properties of rotating pipe flow, in particular tracking several of the most unstable eigenvalues. For moderate Reynolds numbers the azimuthal mode $n = 1$ is found to be the most unstable. We will refer to their work frequently to guide our simulations.

Recently Toplosky & Akylas (1988) did the first work calculating the finite-amplitude waves that arise from the linear instability of rotating pipe flow. These waves are of the form

$$\boldsymbol{v} = \boldsymbol{v}(r, n\theta + \alpha z - ct), \tag{2}$$

and are therefore steady helical waves in an appropriate rotating (or translating) frame. Their numerical work for the fundamental $n = 1$ waves indicates that the surface of spiral waves bifurcates supercritically from the curve of linear stability

lying in the (R_z, R_Ω)-plane of axial and azimuthal Reynolds numbers, i.e. the bifurcating waves will be stable, and the surface they occupy in *Amplitude*-R_z-R_Ω space does not bend toward the zero rotation plane, $R_\Omega = 0$. Their calculations (in which the waves were found by solving the steady three-dimensional Navier–Stokes equations iteratively) were performed in the slow rotation limit of $\alpha \to 0$ and also for $\alpha = 0.1$.

Toplosky & Akylas' results suggest that if steady helical waves exist in non-rotating pipe Poiseuille flow, then they are not directly related to those long waves which exist when the pipe is rotated along its axis at high R_z. This is quite possible as the zero rotation limit is in some sense singular, owing to the loss of the symmetry $(\theta \to -\theta, v_\theta \to -v_\theta)$ once the frame of reference is rotating. Such waves in a stationary pipe are predicted by the high-Reynolds-number asymptotic analysis of Smith & Bodonyi (1982). Using the techniques of nonlinear critical-layer analysis, they found that waves of the form (2) could be constructed, provided $n = 1$ and α and c are determined from the amplitude of the fundamental periodic mode, which is of order $R_z^{-\frac{1}{3}}$. In addition, there is a mean flow correction of order $R_z^{-\frac{1}{6}}$ to the parabolic base flow.

Our computation of the time-dependent Navier–Stokes equations, assuming a helical symmetry for the velocity field

$$\boldsymbol{v} = \boldsymbol{v}(r, \theta + \alpha z, t), \tag{3}$$

is motivated in several ways. As described above, the helical symmetry is the natural one where there is a three-dimensional instability of a swirling axisymmetric base flow. The great advantage of the helical assumption, moreover, is that it allows the definition of helical variables, reducing the equations of motion to two-dimensions, although three-dimensional effects such as vortex stretching are still permitted.

Helical variables were introduced previously by Park, Monticello & White (1984) in the context of simplifying the equations of magnetohydrodynamics. In classical fluid mechanics, there has been some computation of helical fluid flows, though the formulation has been linear and fully three-dimensional, such as for the flow between rotating cylinders, where spiral instability modes are found (Langford *et al.* 1988). On the theoretical side, the existence of slender helical vortex tubes in an inviscid fluid, which are steady in a suitable rotating frame, has been established by Adebiyi (1981). In addition, at large Reynolds numbers the Prandtl–Batchelor results concerning the distribution of vorticity in two-dimensional and axisymmetric steady flows can be extended to those with helical symmetry, using helical variables (Childress, Landman & Strauss 1989).

With our helical Navier–Stokes code, we are able to recalculate the waves found by Toplosky & Akylas, but with an entirely distinct formulation. Using carefully tested and controlled numerical calculations, we have determined that the steady waves of rotating pipe Poiseuille flow undergo a series of bifurcations to other helical states. In particular, waves that have quasi-periodic, period-doubled, and non-periodic (chaotic) time dependence will be described. We are also interested in determining if the waves predicted by Smith & Bodonyi exist in a stationary pipe. Our simulations have been unable to detect such waves, as reported in Landman (1990).

Because the axial wavenumber α is prescribed in the rotating pipe computations, the instabilities found may not be directly observable in the fully three-dimensional system. This is because, in general, other linearly unstable helical waves (with different α) will coexist at given axial and azimuthal Reynolds numbers.

Nevertheless, the behaviour of the system at fixed α is of intrinsic mathematical interest, and also should be observable in an experiment where the wavenumber of the disturbance introduced into a rotating pipe is controllable, as in Fox *et al.* (1968).

In the following section we describe how the helical assumption is exploited to derive the two-dimensional equations of motion in helical variables. In §3 our numerical procedures are described. Our results are presented in §4. This section also includes a simple explanation for the origin of the time-dependent waves found, in terms of the interaction of multiple modes related to the linearized operator of the base flow. In §5 we mention some of the results from our direct simulations of non-rotating pipe flow, and discuss the ramifications of our findings to the instability of Hagen–Poiseuille flow.

2. Formulation

We seek solutions of the equations of motion of a fluid with the helical symmetry (3). This means that in cylindrical polar coordinates (r, θ, z), the physical quantities are functions of r, ϕ, and time t only, where

$$\phi = \theta + \alpha z$$

and α is a real parameter which in inversely proportional to the pitch angle of the helix on which r and ϕ are constant. The helical assumption can be exploited to reduce the fluid equations to two dimensions as follows, as has previously been performed in magnetohydrodynamics (Park *et al.* 1984).

We define $\boldsymbol{h}$ as the Beltrami vector orthogonal to the unit vectors $\boldsymbol{e}_r$ and

$$\boldsymbol{e}_\phi = \frac{\nabla\phi}{|\nabla\phi|} = \frac{\boldsymbol{e}_\theta + \alpha r \boldsymbol{e}_z}{(1+\alpha^2 r^2)^{\frac{1}{2}}}.$$

i.e.
$$\boldsymbol{h} = \frac{r\nabla r \times \nabla\phi}{1+\alpha^2 r^2} = h^2(\boldsymbol{e}_z - \alpha r \boldsymbol{e}_\theta),$$

where
$$h^2 = \frac{1}{1+\alpha^2 r^2}.$$

The helical vector $\boldsymbol{h}$ is found to be divergence free, and thus has the properties

$$\nabla \times \boldsymbol{h} = -2\alpha h^2 \boldsymbol{h}, \quad \nabla \cdot \boldsymbol{h} = 0, \quad |\boldsymbol{h}|^2 = h^2.$$

We decompose the helical velocity and vorticity fields into helical variables such that

$$\boldsymbol{v} = v\boldsymbol{h} + \nabla u \times \boldsymbol{h}, \tag{4a}$$

$$\boldsymbol{\omega} = \zeta \boldsymbol{h} + \nabla\psi \times \boldsymbol{h}. \tag{4b}$$

The four scalar functions on the right-hand side are functions of (r, ϕ, t), and the fields are divergence free because of the property that

$$\boldsymbol{h} \cdot \nabla g = 0 \quad \text{for any } g = g(r, \phi, t). \tag{5}$$

Note that the helical representation can be expanded back into cylindrical polar coordinates and the velocity field (4a) becomes

$$\boldsymbol{v} = \frac{1}{r} u_\phi \boldsymbol{e}_r - h^2(\alpha r v + u_r)\boldsymbol{e}_\theta + h^2(v - \alpha r u_r)\boldsymbol{e}_z.$$

The kinematic condition $\boldsymbol{\omega} = \boldsymbol{\nabla} \times \boldsymbol{v}$ implies that

$$\psi = v, \quad -h^2\zeta = \Delta^* u + 2\alpha h^4 v, \tag{6}$$

where $$\Delta^* u = \boldsymbol{\nabla} \cdot h^2 \boldsymbol{\nabla} u = \frac{1}{r}\frac{\partial}{\partial r}\left(r h^2 \frac{\partial u}{\partial r}\right) + \frac{1}{r^2}\frac{\partial^2 u}{\partial \phi^2}$$

is the helical Laplacian operator.

The aim is to find the evolution equations for the helical velocity and vorticity components v and ζ. We consider the momentum equation of an incompressible fluid of density ρ and kinematic viscosity η in a frame rotating with constant angular velocity $\boldsymbol{\Omega}_0 = \Omega_0 \boldsymbol{e}_z$:

$$\frac{\partial \boldsymbol{v}}{\partial t} + \boldsymbol{v} \cdot \boldsymbol{\nabla} \boldsymbol{v} + 2\boldsymbol{\Omega}_0 \times \boldsymbol{v} = -\boldsymbol{\nabla}(p/\rho - \tfrac{1}{2}\Omega_0^2 r^2) + \eta \nabla^2 \boldsymbol{v},$$

$$\boldsymbol{\nabla} \cdot \boldsymbol{v} = 0.$$

We also consider the evolution of the vorticity by taking the curl of this equation. Forming the scalar product of each of these equations with $\boldsymbol{h}$, and using (4), one finds

$$h^2 \frac{\partial v}{\partial t} = h^2 \boldsymbol{h} \cdot (\boldsymbol{\nabla} u \times \boldsymbol{\nabla} v) + \eta(\Delta^* v + 2\alpha h^4 \zeta) + 2\Omega_0 h^2 (\boldsymbol{e}_z \cdot \boldsymbol{\nabla} u) - \boldsymbol{h} \cdot \boldsymbol{\nabla} p/\rho, \tag{7a}$$

$$h^2 \frac{\partial \zeta}{\partial t} = -2\alpha h^4 \boldsymbol{h} \cdot (\boldsymbol{\nabla} u \times \boldsymbol{\nabla} v) + \boldsymbol{h} \cdot (\boldsymbol{\nabla} h^2 v \times \boldsymbol{\nabla} v) - \boldsymbol{h} \cdot (\boldsymbol{\nabla} h^2 \zeta \times \boldsymbol{\nabla} u)$$
$$+ \eta \Delta^* \zeta - 2\alpha h^2 \eta (2\alpha h^4 \zeta + \Delta^* v) - 2\Omega_0 \boldsymbol{h} \cdot \boldsymbol{\nabla} \times (\boldsymbol{e}_z \times v \boldsymbol{h}), \tag{7b}$$

where we have used the identities (5), (6) and $\boldsymbol{h} \cdot (\boldsymbol{\nabla} \times (\boldsymbol{h} \times \boldsymbol{\nabla} g)) = \Delta^* g$ for any helical variable g.

The pressure term in (7a) vanishes if we assume that p also maintains helical symmetry – however, we retain it in our study because the Poiseuille flow will be maintained by a pressure gradient in the z-direction, which will act as a forcing in the momentum equation.

The geometry we consider is a circular pipe of radius r_0, rotating along its axis of symmetry $\boldsymbol{e}_z$ with angular velocity Ω_0. On imposing a uniform pressure gradient $-Q_0$, a viscous fluid undergoing laminar Poiseuille flow superimposed on solid-body rotation will maintain a parabolic velocity profile

$$\boldsymbol{v} = U_0(1 - r^2/r_0^2)\,\boldsymbol{e}_z + r\Omega_0 \boldsymbol{e}_\theta \tag{8}$$

as viewed in an inertial frame, with maximum centreline velocity

$$U_0 = \frac{Q_0 r_0^2}{4\rho\eta}.$$

Non-dimensionalizing all quantities with respect to r_0 and U_0, we define

$$R_z \equiv \frac{1}{\nu} \equiv \frac{U_0 r_0}{\eta}, \quad R_\Omega \equiv \frac{\Omega_0 r_0^2}{\eta}, \quad \Omega \equiv \frac{\Omega_0 r_0}{U_0}.$$

ν is the inverse of the axial Reynolds number R_z, R_Ω is the azimuthal Reynolds number, and Ω is the inverse Rossby number. The two dimensionless measures of the rotation rate are related by

$$R_\Omega = \Omega R_z. \tag{9}$$

At different times it will be convenient to use either Ω or R_Ω, the latter being the more common in the literature (note that the azimuthal Reynolds number is sometimes given the symbol Ω elsewhere, and that non-dimensionalizations of the velocity field can vary in the literature).

The non-dimensional form of the base flow becomes $\boldsymbol{v} = (1-r^2)\boldsymbol{e}_z + r\Omega\boldsymbol{e}_\theta$. In the rotating frame the azimuthal component of velocity disappears, and the no-slip boundary conditions are satisfied at $r = 1$.

With this scaling the equations of motion (7) can be written

$$\frac{\partial v}{\partial t} = J(u,v) + \nu(h^{-2}\Delta^* v - 2\alpha w - 4\alpha^2 h^4 v) + [4\nu + 2\alpha\Omega u_\phi], \tag{10a}$$

$$\frac{\partial w}{\partial t} = J(u,w) + 2\alpha h^4 J(u,v) + 2\alpha^2 h^4 Y(u,v) + \nu\Delta^*(h^{-2}w + 2\alpha h^2 v) + [-8\alpha h^4\nu - 2\alpha h^2\Omega(v_\phi + 2\alpha h^2 u_\phi)], \tag{10b}$$

$$\Delta^* u = w. \tag{10c}$$

The nonlinear terms above are given by

$$J(u,v) = \frac{1}{r}(u_r v_\phi - v_r u_\phi), \quad Y(u,v) = v(v_\phi + 4\alpha h^2 u_\phi).$$

The evolution equation for w has been obtained by adding (7b) to $2\alpha h^2$ times (7a).

The equations (10) describe the helical motions of a fluid in rotating pipe flow, which are to be solved numerically. The no-slip boundary conditions on the wall of the pipe are

$$v = u = u_r = 0 \quad \text{at } r = 1.$$

The bracketed term in each equation comes from the pressure forcing and the Coriolis force. In the event that there is no external pressure gradient, the former terms proportional to ν are dropped, and the equations must be non-dimensionalized with respect to some other characteristic velocity (e.g. from initial conditions). We will assume here that the flow is always being driven by a pressure gradient, however.

It is important to note that the Reynolds number R_z is based on the pressure gradient, and not the mass flux. Although this distinction is irrelevant for the base flow, for unsteady nonlinear flows these measures of the mean flow can have different time dependence.

The basic laminar state of the system, which exists for all axial and azimuthal Reynolds numbers, is given in the rotating frame in non-dimensional helical variables by

$$\left.\begin{aligned} v = 1-r^2, \quad u = \tfrac{1}{4}\alpha(1-2r^2+r^4), \quad w = -2\alpha h^4(1-2r^2-\alpha^2 r^4), \\ \zeta \equiv -h^{-2}(w + 2\alpha h^4 v) = -2\alpha r^2. \end{aligned}\right\} \tag{11}$$

The equations (10) reduce to the usual equations of motion for two-dimensional flow when $\alpha = 0$, with v and w the axial velocity and vorticity respectively, and u the stream function in polar coordinates. In the (singular) limit $\alpha \to \infty$, (10) reduce to the axisymmetric equations of motion with the rescaling $\tilde{v} = v/\alpha, \tilde{u} = u/\alpha$, in which case $\tilde{u}$ is the Stokes stream function and $\tilde{v}/r$ is the swirl velocity.

3. Numerical method

The computer code is based on a finite difference method in the radial direction, and a spectral method in the angular (ϕ) direction. We assume solutions of the equations (10) are 2π-periodic in $\phi = \theta + \alpha z$, and take a finite Fourier transform

$$v(r,\phi) = \sum_{m=-M}^{M} \hat{v}_m(r)\, \mathrm{e}^{\mathrm{i}m\phi},$$

and similarly for u and w. In the computations modes $m \geqslant 0$ need only be considered as $\hat{v}_{-m} = \hat{v}_m^*$.

We are able to compute solutions for any azimuthal wavenumber corresponding to an instability of mode n in (1), as modes $1 \leqslant m \leqslant n-1$ will remain zero if initially zero. Almost all of our calculations have all modes excited, however, corresponding to the instability of the fundamental azimuthal mode $n = 1$.

The equations of motion in Fourier space become

$$\frac{\partial \hat{v}_m}{\partial t} = \hat{J}_m(\hat{u},\hat{v}) + \nu h^{-2} \mathrm{L}_0 \hat{v}_m + \nu(4 + 2\mathrm{i}m\alpha R_\Omega \hat{u}_m) + \{-2\alpha\nu(\hat{w}_m + 2\alpha h^4 \hat{v}_m) - \nu m^2 (rh)^{-2} \hat{v}_m\}, \quad (12a)$$

$$\frac{\partial \hat{w}_m}{\partial t} = \hat{J}_m(\hat{u},\hat{w}) + 2\alpha h^4 \hat{J}_m(\hat{u},\hat{v}) + 2\alpha^2 h^4 \hat{Y}_m(\hat{u},\hat{v}) + \nu \mathrm{L}_0(h^{-2}\hat{w}_m + 2\alpha h^2 \hat{v}_m) + \nu(-8\alpha h^4 - 4\mathrm{i}m\alpha^2 h^4 R_\Omega \hat{u}_m) + \{-\nu(m^2 r^{-2}(h^{-2}\hat{w}_m + 2\alpha h^2 \hat{v}_m) - 2\mathrm{i}m\nu\alpha R_\Omega h^2 \hat{v}_m\}, \quad (12b)$$

$$\mathrm{L}_0 \hat{u}_m - m^2 r^{-2} \hat{u}_m = \hat{w}_m, \quad (12c)$$

with

$$\mathrm{L}_0 = \frac{1}{r}\frac{\mathrm{d}}{\mathrm{d}r}\left(rh^2 \frac{\mathrm{d}}{\mathrm{d}r}\right).$$

$\hat{J}_m$ and $\hat{Y}_m$ are the transforms of the nonlinear terms, which are evaluated pseudospectrally (i.e. multiplication is performed in real space) with fast Fourier transforms – dealiasing is available and used to check computations. Note that only 6 products need be evaluated to calculate the nonlinearity, as opposed to the 11 products required by a three-dimensional primitive variable formulation.

The linear terms not involving derivatives in the modal equations (12) (those inside the curly braces) are integrated 'exactly', by performing a similarity transformation on the solution vectors $\boldsymbol{x} = (\hat{v}_m^k, \hat{w}_m^k)$, i.e. we write each of the modal equations as

$$\boldsymbol{x}_t = \boldsymbol{A}\boldsymbol{x} + f(\boldsymbol{x}, t)$$

at $r = k\Delta r$, where $\boldsymbol{A}$ is the complex 2×2 matrix of the coefficients of $\hat{v}_m^k$ and $\hat{w}_m^k$ in the braced terms in (12). Letting $K^{-1}\boldsymbol{A}K = \Lambda$ be the diagonalization of $\boldsymbol{A}$, we have

$$\frac{\mathrm{d}}{\mathrm{d}t}[\mathrm{e}^{-\Lambda t} K^{-1} \boldsymbol{x}] = \mathrm{e}^{-\Lambda t} K^{-1} f(\boldsymbol{x}, t).$$

This can then be discretized in time with whatever stepping scheme we choose, so that for example with second-order Adams–Bashforth time stepping

$$\boldsymbol{x}^{n+1} = K\,\mathrm{e}^{-\Lambda\Delta t} K^{-1}[\boldsymbol{x}^n + \tfrac{1}{2}\Delta t(3f(\boldsymbol{x}^n, t^n) - K\,\mathrm{e}^{-\Lambda\Delta t} K^{-1} f(\boldsymbol{x}^{n-1}, t^{n-1}))].$$

Using such an explicit method with a second-order finite-difference scheme in the radial direction, the stability restriction on the viscous terms requires that $\delta t \lesssim (\Delta r)^2/\nu$, which is far less restrictive than the condition $\delta t \lesssim (\Delta r)^2/\nu M^2$ which would otherwise hold.

The finite differences in the radial direction are second order centred on a stretched grid, allowing a concentration of points in the boundary layer for high-Reynolds-number flows. The stretching function is that used by Chesshire & Henshaw (1989), and is of the form

$$x(r) = \left[r + \sum_{i=1}^{n_U} [U_i(r) - U_i(0)] + \sum_{j=1}^{n_V} [V_j(r) - V_j(0)]\right] s_1, \tag{13}$$

where $$U_i(r) = \tfrac{1}{2} a_i \tanh b_i (r - c_i)$$

clusters points around point $r = c_i$ (e.g. at the boundary $r = 1$), and

$$V_j(r) = \frac{d_j - 1}{2e_j} \log\left[\frac{\cosh e_j (r - f_j)}{\cosh e_j (r - f_{j+1})}\right]$$

permits a transition to a uniform concentration of mesh points between f_j and f_{j+1}, with a spacing d_j times less than where the linear term in (13) is dominant. s_1 is chosen so that $x(1) = 1$. Most often at moderate Reynolds numbers only stretching in the boundary layer is used (e.g. $n_U = 1$, $n_V = 0$, $a_1 = 1$, $b_1 = 4$, $c_1 = 1$). However, at fast rotation when centre-modes appear, a stretching V_1 is also included so that a finer mesh is incorporated at the origin. In the computations smoothness in the radial direction is checked *a posteriori* by plotting profiles of the individual modes or contours of the solution in the (r, ϕ)-plane.

Several timestepping schemes were tested. As shown above, the second-order Adams–Bashforth method is used in general, with the Heun (second-order Runge–Kutta) method used as an initial step. Because of the similarity transform technique, for flows at the moderately high R_z we have computed, the stability restriction on the timestep coming from the viscous terms is usually of the same order as that of the CFL stability condition (Richtmeyer & Morton 1967) from the convective terms, and thus the more costly and difficult-to-implement implicit schemes were found unnecessary. In our computations the CFL condition is monitored and the timestep refined accordingly.

We illustrate the algorithm used on a uniform radial grid $[r_k = k/N, k = 0 \ldots N+1\}$. Given $(\hat{v}_m^k, \hat{u}_m^k, \hat{w}_m^k)$ on $0 \leqslant k \leqslant N$ for each mode $0 \leqslant m \leqslant M$, the equations (12*a*) and (12*b*) are stepped forward in time on the internal grid points $0 \leqslant k \leqslant N-1$. For the $m = 0$ mode a Neumann condition is used at the origin; for modes $m > 0$ all radial functions are set equal to zero for $k = 0$. The elliptic equation (12*c*) is now solved subject to the Dirichlet condition on u, for each radial function $\hat{u}_m$ on the grid points $0 \leqslant k \leqslant N-1$. The $(M+1)LU$ factorizations of the tridiagonal Laplacians are calculated initially and stored. On setting $\hat{v}_m^N = \hat{u}_m^N = 0$ and $\hat{u}_m^{N+1} = \hat{u}_m^{N-1}$ from the no-slip boundary conditions, the vorticity at the boundary is updated from applying equation (12*c*) at $k = N$. This completes one timestep.

When the radial grid is stretched by a smooth function $x(r)$, the above procedure is carried out on the uniform grid $\{x_k\}$, with suitable modifications made to the difference formulae using the functions $x'(r)$ and $r(x)$ (the latter is tabulated at the grid points using Newton's method).

It is worth noting here that the above numerical method was chosen after the initial failure of a modified finite-difference method, which made use of the fact that the leading-order behaviour of each Fourier-helical mode m is r^m at the origin, by factoring this out of the computational solution. This method generated numerical instabilities at the origin in the high m modes, however, which were easily detected as the energy of these modes increased without bound. These spurious modes could

not be controlled despite the use of implicit timestepping schemes for the linear terms, or alternatively predictor–corrector methods. No instability at the origin was detected in the current method, given a timestep which was sufficiently small by the criterion outlined above. The smoothness of the solution at the origin was frequently checked by plotting radial modes at a series of times throughout a simulation.

During the computations, the following energies are monitored:

$$E_m^{(v)} = \int_0^1 |\hat{v}_m(r)|^2 r\,\mathrm{d}r, \quad E^{(v)} = \sum_{m=1}^{M} E_m^{(v)},$$

as well as the analogous quantities for u and w. Provided $\log E_m^{(w)}$ decayed linearly as a function of m (i.e. exponential decay of the solution in Fourier space), the calculations were found to be resolved adequately in the azimuthal direction. This observation was tested by the addition of more modes and by dealiasing the code, and corroborates the conclusions of Marcus (1981) for simulations of thermal convection. Like Marcus, we found that complicated time-dependent behaviour could arise in an under-resolved simulation (indicated by an increasing tail on the Fourier spectrum), which then reverted to being simply periodic with the addition of sufficient helical modes.

Also the non-dimensional mass flux perturbation

$$\Phi = 4\int_0^1 (\hat{v}_0 + 2\alpha h^2 \hat{u}_0)\, h^2 r\,\mathrm{d}r - 1,$$

the circulation averaged over the pipe radius

$$\Gamma = \frac{3}{\Omega}\int_0^1 h^2(\alpha r\hat{v}_0 + \hat{u}_0')\, r\,\mathrm{d}r,$$

and the kinetic energy of the helical motion

$$E = \frac{4}{(\frac{1}{3}+\frac{1}{2}\Omega^2)}\sum_{m=1}^{M}\int_0^1 \left[h^2(|\hat{v}_m|^2 + |\hat{u}_m'|^2) + \frac{m^2}{r^2}|\hat{u}_m|^2\right] r\,\mathrm{d}r, \tag{14}$$

can be measured (and are equivalent to those of Toplosky & Akylas 1988), all vanishing for the basic axisymmetric flow (11). The mass flux perturbation provides the relationship between the mass flux Reynolds number R_D and the pressure Reynolds number R_z, such that

$$\frac{R_D - R_z}{R_z} = \Phi. \tag{15}$$

Pointwise quantities such as the helical velocity $v(r,\phi)$ at a fixed point inside the pipe are also monitored. The power spectra of this and the global quantities above can be computed, and used as diagnostics for the character of the flow.

The correctness of the code was tested by picking time-periodic functions $v^T(r,\phi,t)$ and $u^T(r,\phi,t)$, satisfying the no-slip boundary conditions. On substituting these into the equations of motion, the resulting residuals (calculated analytically) were used as forcing functions for the equations in the numerical integration. The error of the forced numerical solutions could then be measured against the true solutions chosen. In this way the method was shown to be second order in space and time.

Also, by integrating small perturbations to the base flow for long times, the linear growth/decay rate and also the phase speed of the dominant least-stable eigenmode were computed. This was done by plotting $\log E^{(v)}$ and also the pointwise velocity (normalized with the energy) versus time. In the non-rotating pipe, the values obtained were in good agreement (within 1%) with the eigenvalue calculations of

Salwen, Cotton & Grosch (1980) for the $m = 1$ mode, and with Salwen & Grosch (1972) for $m > 1$.

4. Numerical results

In all the simulations of rotating pipe flow that we discuss, initial transients are ignored, and only stable solutions of the Navier–Stokes equations are studied. The transients omitted are typically of the length of the (fast) advective timescale for the helical modes, but of order $1/R_z$ for the mean flow, given an initial condition at a neighbouring solution in parameter space.

We first compare our computations with the steady wave calculations of Toplosky & Akylas (1988). In part of that study, they fixed $\alpha = 0.1, R_\Omega = -415.5$ (the rotation necessary for instability with the least amount of axial flow), and increased R_z past the minimum critical value of 83. Once the base flow becomes unstable, a helical wave is set up in the pipe, which rotates at an angular velocity f_1 relative to an observer rotating with the pipe angular velocity $\Omega = R_\Omega/R_z$ (computations in our rotating frame thus yield pointwise velocities of period $2\pi/f_1$). However, the wave is of constant shape and energy, and is steady in a frame rotating at angular velocity $\Omega + f_1$, which is not known *a priori*.

In the rotating frame, all the steady waves we have computed have an angular velocity $f_1 > 0$ (for $\Omega < 0$). This observation is corroborated by the discussion of Cotton & Salwen (1981) on the phase speed of helical waves from linear theory. The growth rate σ is their paper is related to f_1 by $\mathrm{Im}\,\sigma = R_z(f_1 + \Omega)$ (allowing for a difference in sign for α and Ω in their study). In the inertial frame the solutions are a periodic function of $(\theta - \Omega t - \alpha c_r t) + \alpha z$, so that $f_1 = \alpha c_r$. Cotton & Salwen find that $0 \leqslant c_r \leqslant 1$ for all the linearly unstable modes they computed. This result corresponds to the existence of a critical layer at $r_c = (1 - c_r)^{\frac{1}{3}}$ in the inviscid stability equations, and puts a bound on the angular velocity (phase speed) of such waves.

Thus, in the rotating frame, a simple helical wave rotates counter to the direction of rotation ($f_1 \Omega < 0$); however, in a fixed frame, the velocity $f_1 + \Omega$ can have either sign, and as observed by Cotton & Salwen, the wave rotation is counter to the swirl in the slow rotation regime, and with the swirl in the fast rotation regime.

We computed the averaged quantities mass flux, energy and circulation of the (temporally stable) solutions at various R_z between 83 and 600. For axial Reynolds number less than 300 there is rough agreement between our results and those of Toplosky & Akylas. For example, at $R_z = 300$, we quote our results with Toplosky & Akylas's in parentheses:

$$\Phi = -0.167 \quad (-0.183), \quad \Gamma = -4.62 \times 10^{-3} \quad (5 \times 10^{-3}),$$
$$E = 3.41 \times 10^{-3} \quad (4.5 \times 10^{-3}).$$

The difference in sign in the circulation integral appears to be an error, as the helical wave calculated depletes the vorticity of the solid-body rotation, as it does the mass flux. The explanation for the quantitative discrepancy probably lies in the disclaimer made by Toplosky & Akylas themselves: inadequate resolution due to only 4 Fourier modes (i.e. $M = 4$). We found that at $R_z = 300$, $M = 7$ resulted in an inverted energy spectrum leading to inflated values of the averaged quantities above. The problem was alleviated by taking $M = 15$. Radial resolution used was $N = 50$, with boundary-layer stretching to reduce the vorticity gradient at $r = 1$.

Steady wave profiles are shown in figures 1 and 2 for the above values $R_\Omega = -415.5$ and $\alpha = 0.1$, at $R_z = 100$ and $R_z = 300$ respectively. In this regime global quantities

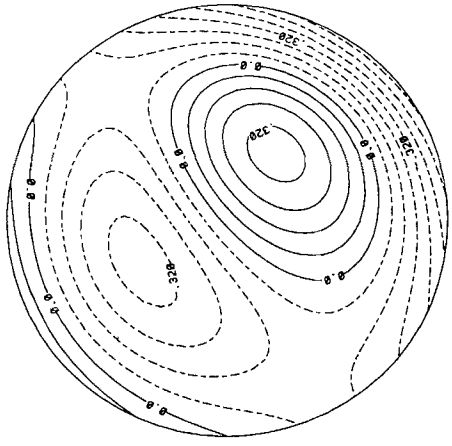

FIGURE 1. Contours of the steady rotating helical vorticity ζ, $R_z = 100$, $R_\Omega = -415.5$, $\alpha = 0.1$. ——, positive values; – – –, negative values.

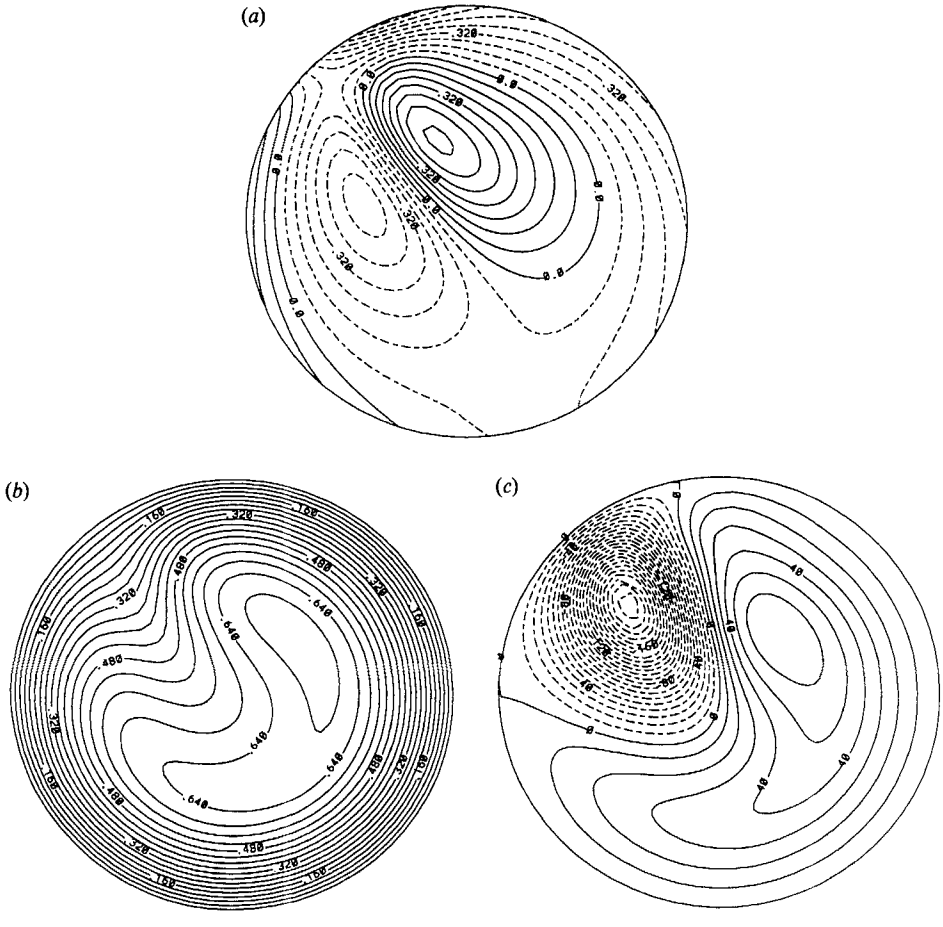

FIGURE 2. Contours of the steady rotating wave, $R_z = 300$, $R_\Omega = -415.5$, $\alpha = 0.1$. (*a*) Vorticity ζ. (*b*) Helical velocity v. (*c*) v with the mean flow subtracted out ($v - v_0$).

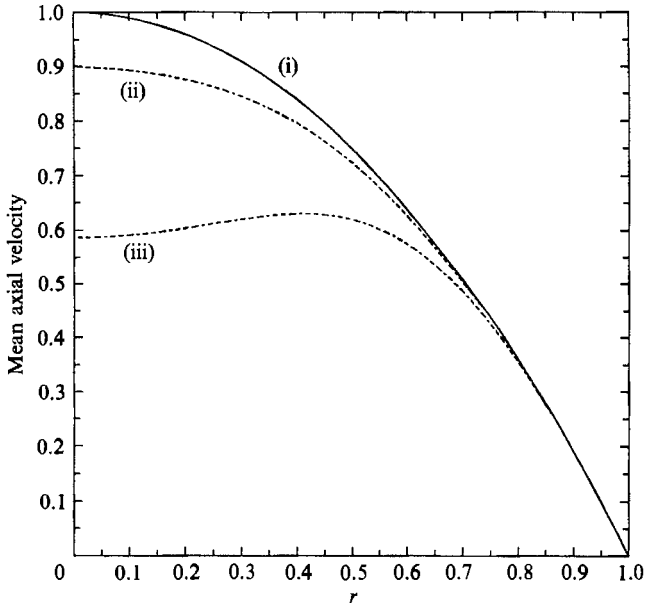

FIGURE 3. Mean axial flow profiles for the steady waves of figures 1 and 2. The solid line (i) is the parabolic profile, stable up to $R_z = 83$; (ii) $R_z = 100$; (iii) $R_z = 300$.

such as the energy and mass flux of the waves are steady in time, whereas the velocity at a fixed station in the pipe will be simply periodic (except at the origin, where it is steady). Figures 1 and 2(*a*) are contours of the helical vorticity $\zeta(r, \phi)$ $(0 \leqslant r \leqslant 1, 0 \leqslant \phi \leqslant 2\pi)$ at the two different axial Reynolds numbers. Such plots can be thought of as a cross-section of the flow in the pipe at a fixed station in z. Figure 2(*b*) shows contours of the helical velocity $v(r, \phi)$, and (*c*) plots v with the mean flow removed. As α is relatively small, the direction of these quantities is out of the plane with a slight clockwise tilt. The waves rotate steadily in the rotating frame, with a period $(2\pi/f_1)$ of 96 and 104 respectively, which is slow compared to the pipe rotation time of 1.51 and 4.54 at these different values of R_z.

We observe that the waves consist of an oppositely signed helical vortex pair, in comparison with the base flow for which ζ is everywhere negative. This generation of positive vorticity is responsible for the property that the vortex tends to rotate slower than the underlying base flow of solid-body rotation. With increased axial flow the steady wave becomes more nonlinear, and departs from the mostly $m = 1$ symmetric perturbation seen at the lower Reynolds number.

Looking now at the contours of the helical velocity v, the axisymmetric base flow has been considerably distorted, and when the underlying time-independent mean flow is subtracted out (figure 2*c*), we see that a strong jet of fluid moving counter to the base Poiseuille flow has been set up, thus depleting the axial flow. To illustrate this explicitly, the mean axial flow $h^2(v_0 - \alpha r u_0')$ is plotted against r in figure 3. At $R_z = 300$, the mass flux is depleted 17% and the mean axial velocity has developed an inflexion point and is quite flat. Although the flow is a long way from being turbulent, it is interesting that these are characteristics of the profile observed in turbulent pipe flow (Wygnanski & Champagne 1973).

By increasing R_z from 300 to 400, a qualitative change from the steady waves of Toplosky & Akylas occurs in our simulations. The steady rotating wave undergoes an instability, such that the energy goes from being steady to simply periodic in time,

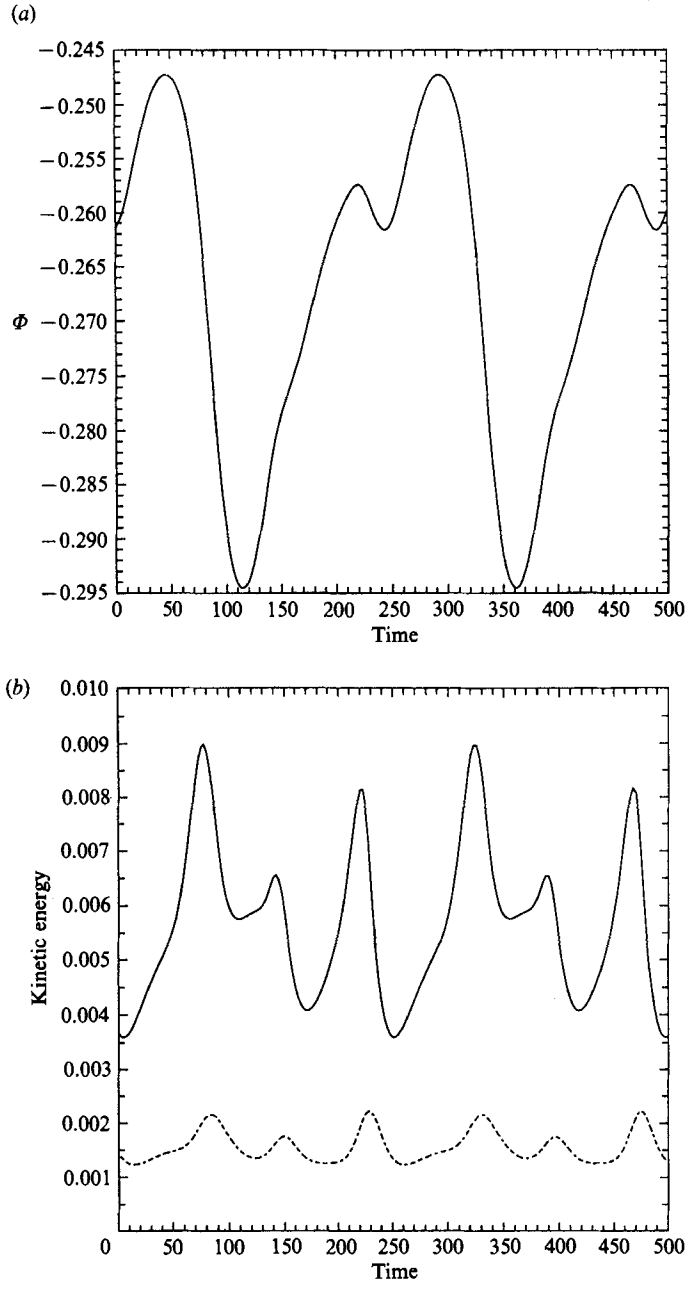

FIGURE 4. Time periodic global quantities for the wave at $R_z = 600$, $R_\Omega = -415.5$, $\alpha = 0.1$. (*a*) Mass flux perturbation. (*b*) Kinetic energy ——, parallel and – – –, perpendicular to the helical direction.

and the pointwise velocity changes to quasi-periodic with two independent frequencies. This indicates the presence of a second Hopf bifurcation leading to two oscillatory modes (the initial bifurcation from the parabolic base flow to a rotating wave can also be considered to be Hopf bifurcation by an observer in the inertial frame).

Figures 4 plot the time-periodic mass flux and kinetic energy of the waves over two of these cycles of period 245. In figure 4 (*b*) the energy, defined in (14), has been split

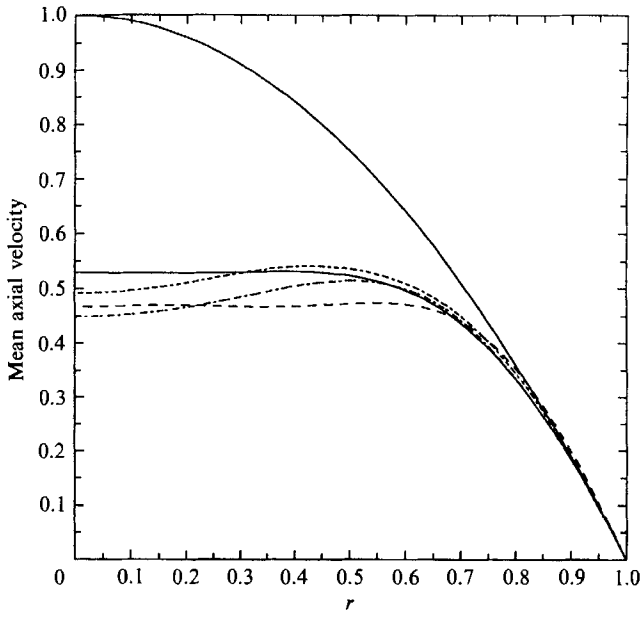

FIGURE 5. Mean axial flow profiles at various times over one cycle for the wave at $R_z = 600$, $R_\Omega = -415.5$, $\alpha = 0.1$. The profile for the parabolic basic flow is also shown.

into its two components, one parallel (depending only on v) and the other perpendicular (depending on u) to the helical direction **h**. We observe that most of the kinetic energy resides in the direction of the helix, and there is no apparent transfer of energy between the two directions. The mean flow profile in figure 5 is fairly flat as it was in the steady regime, although now it fluctuates periodically in time as shown.

We have been able to make colour animations of such flows, which aid in identifying the vortex dynamics involved, as described below. In figure 6, the contours of helical vorticity are plotted at various times within a cycle of the oscillation, at $R_z = 600$. The four plots have been reoriented in order that the vorticity dynamics can be elucidated more clearly. The simplest state is that of a pair of vortices, shown at time 0. By time 70 the positive vortex has elongated, and as the new extremity of this vortex approaches the wall, there is an enhancement of vorticity due to vortex stretching. This part of the vortex becomes dominant, and at times 100 and 130 we observe a folding action of the positive vorticity and this new vortex annihilates a weaker vortex pair. By time 150 the configuration is again that of a single vortex pair, slightly different from that at time 0. A similar, though less dramatic, stretching, folding, and annihilation event takes place from time 150 to 245, when the original flow is again recovered (though in a different orientation within the pipe). Throughout this process the negative vortical structures appear to play only a passive role, with the main negative vortex remaining almost constant in shape.

We have not computed at axial Reynolds numbers greater than 600 for $\alpha = 0.1$, $R_\Omega = -415.5$, owing to the prohibitive expense of such calculations, caused by the relatively large advective timescales at small α and long transients. We did, however, check that in the slow rotation regime the bifurcation to steady waves is supercritical, as found by Toplosky & Akylas, by evolving small perturbations to the

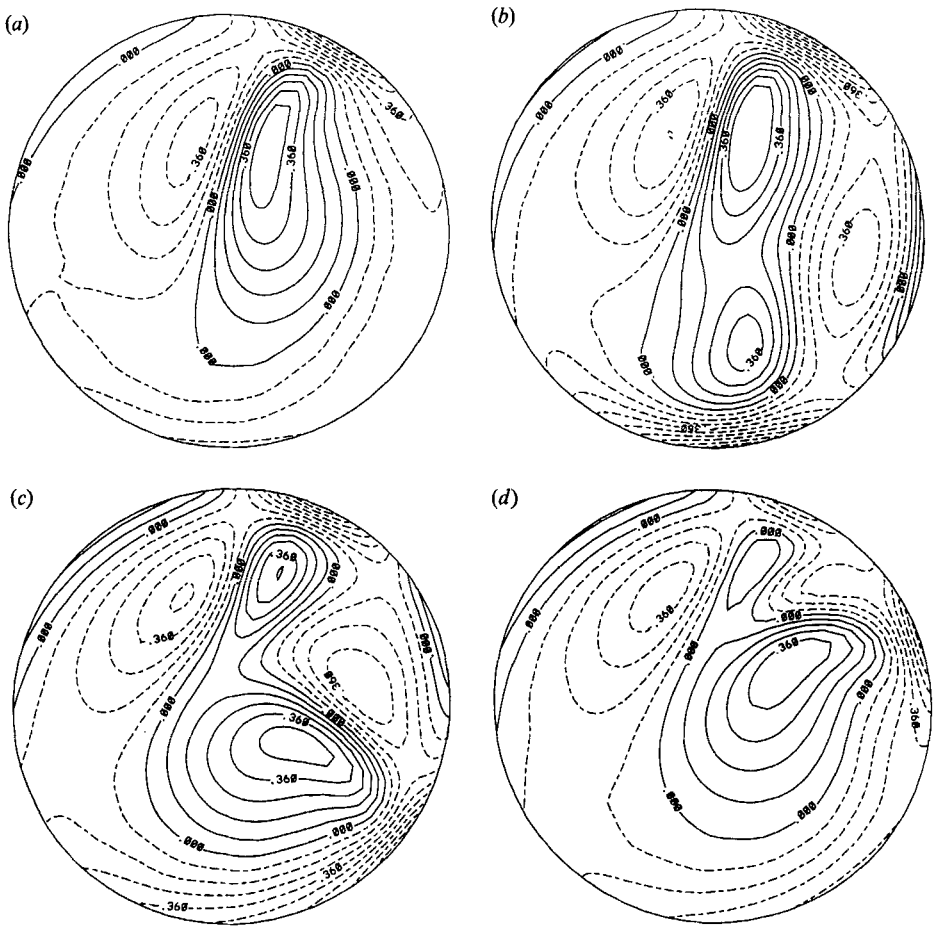

FIGURE 6. Contours of helical vorticity ζ, at times (*a*) $t = 0$, (*b*) $t = 70$, (*c*) $t = 100$, (*d*) $t = 130$; $R_z = 600$, $R_\Omega = -415.5$, $\alpha = 0.1$. The period of one cycle is 245. Each contour plot has been rotated to ease identification of the vortical structures.

base flow at $R_z = 1000$, $\alpha = 0.1$ for rotation rates in the neighbourhood of the bifurcation point $R_\Omega = -28$. Such a result is important as it runs contrary to the conjecture that waves in a slowly rotating pipe have continuations to helical equilibria in Hagen–Poiseuille flow (in fact Toplosky & Akylas find that the bifurcation becomes more supercritical as R_z increases).

The second set of computations we describe was performed with $\alpha = 1.0$ and $\Omega = -0.5$, at an increasing sequence of R_z. In this case we can think of fixing the wavenumber of the disturbances and reducing the viscosity of the fluid, instead of increasing the centreline velocity (as in the case when R_Ω is fixed). In figure 7 the marginal stability curves are shown in the (R_z, Ω)-plane for $\alpha = 1$ and the azimuthal index $n = 1$, using the data from figure 12 of Cotton & Salwen (1981) in the (R_z, R_Ω)-plane and the relationship (9). As R_z is increased we see that it is possible to destabilize more than one mode from the linear theory. Furthermore, the region of parameter space illustrated lies close to a point where a degenerate bifurcation occurs (when the bounded region of two unstable modes disappears at $\Omega \approx -0.5$, $\alpha \approx 1.1$). The amplitude equations at this double Hopf bifurcation were studied by Mahalov & Leibovich (1988), who indicate that complex dynamical behaviour can be expected

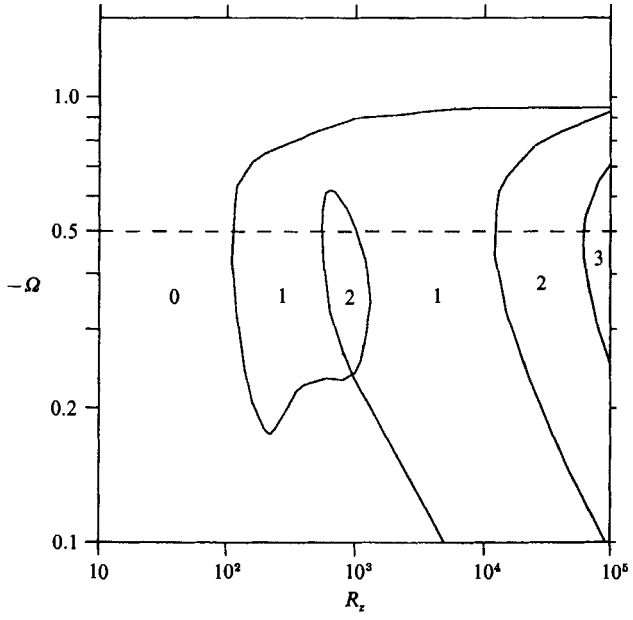

FIGURE 7. Neutral stability curves for the lowest eigenmodes of rotating Poiseuille flow, $n = 1$, $\alpha = 1.0$. The numbers refer to the number of unstable modes in each region (data from Cotton & Salwen 1981). Simulations were performed along the line $\Omega = -0.5$.

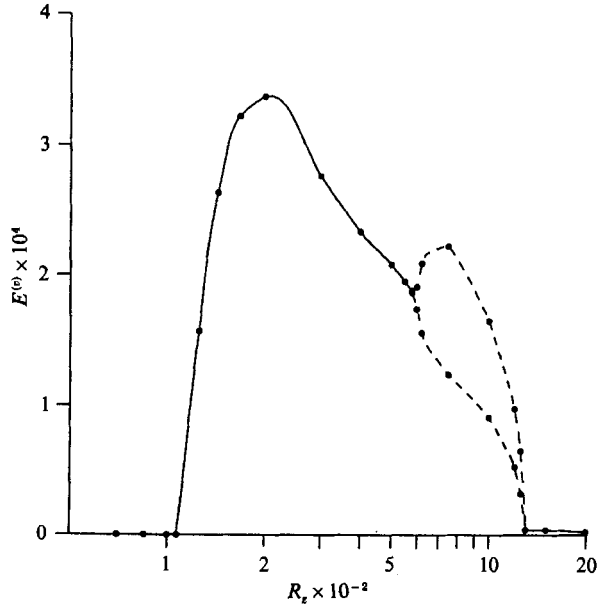

FIGURE 8. Bifurcation diagram for helical waves with $\Omega = -0.5$, $\alpha = 1.0$. ——, steady rotating waves; – – –, the envelope of the amplitude of waves with time-periodic energy.

near this point in parameter space. Figure 7 also illustrates the property that the pipe rotation rate Ω required to destabilize the flow tends to zero like $R_z^{-\frac{1}{2}}$ as the axial flow is increased.

Figure 8 is a bifurcation diagram plotting the energy $E^{(v)}$ versus R_z for the helical waves we have computed with our fully nonlinear time-dependent code, along the

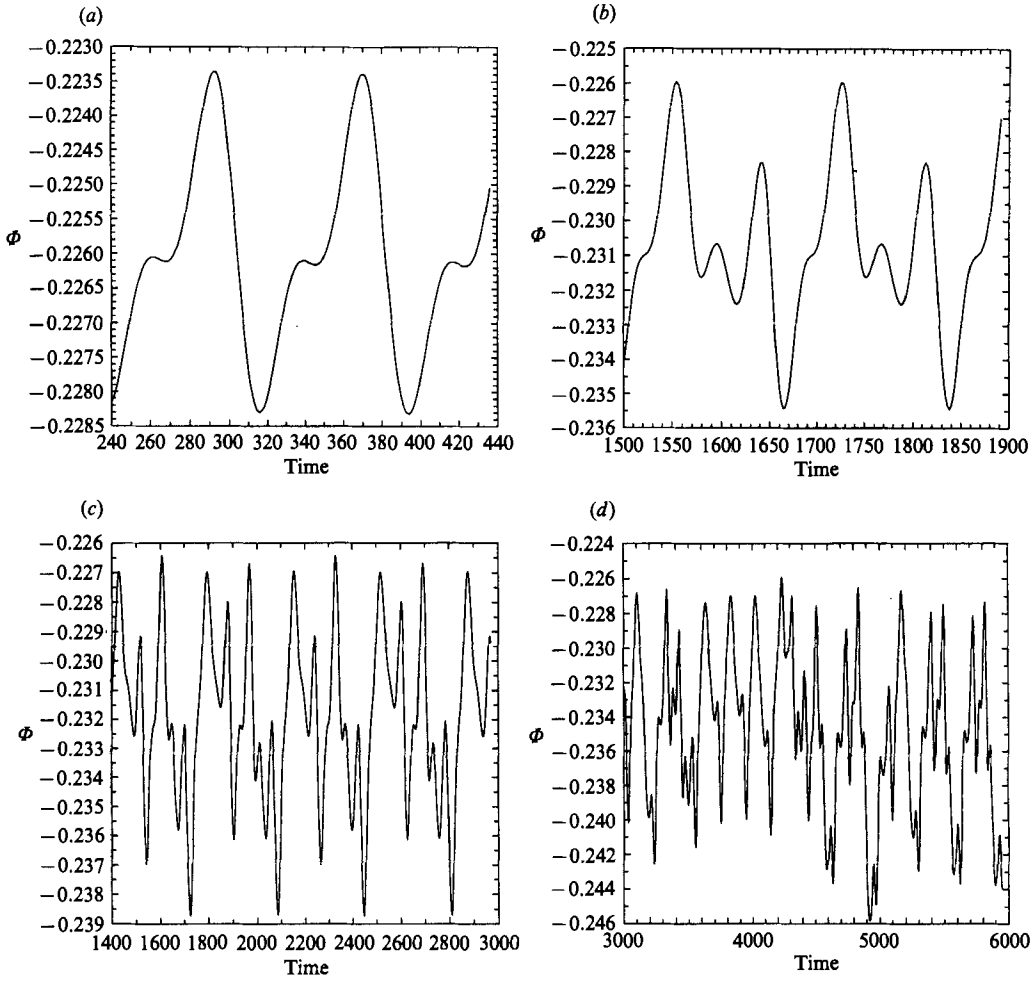

FIGURE 9. Time traces of the mass flux perturbation as the pitch of the helical waves is increased, $R_z = 500$, $\Omega = -0.5$. (*a*) $\alpha = 0.3$, after one Hopf bifurcation. (*b*) $\alpha = 0.275$, after the first period doubling. (*c*) $\alpha = 0.265$, soon after two further doublings. (*d*) $\alpha = 0.25$, non-periodic regime. Note that the timescales on the graphs differ, and that transients are not shown.

ray on which $\Omega = -0.5$, $\alpha = 1$. Starting from $R_z = 107$, the basic flow becomes unstable supercritically and a steady helical wave is set up, rotating at an angular velocity $f_1 > 0$, analogous to that already described. At $R_z = 580$, we once again find an instability to a two-periodic velocity field in the pipe. The unsteady waves persist past $R_z = 1000$, but by $R_z = 1500$ singly periodic flow is once again achieved. As R_z is increased further, the helical waves decrease in amplitude and appear to be evolved from linearly unstable centre modes; we have not studied this regime comprehensively owing to the sensitivity of the calculations at high Reynolds numbers.

The above bifurcation phenomena is seen to have a simple explanation in terms of the known linear stability results for rotating pipe flow. From figure 7 we see that there are two unstable eigenmodes for $\Omega = -0.5$ for R_z in the interval (560, 1100). Because the underlying mean flow is not significantly modified by the nonlinear waves in this parameter regime (for example, the mass flux is at most depleted 4%), the linear stability theory for the parabolic base flow remains relevant. This results

in the window of secondary instability, in which two independent helical modes oscillate at frequencies f_1 and f_2. By computing power spectra of the pointwise velocity $v(r = 0.5, \phi = 0)$ in the quasi-periodic region, two peaks at independent frequencies f_1 and f_2 are easily identified, the peak at f_2 growing in amplitude as R_z is increased past the secondary bifurcation point. Linear eigenvalue computations confirm that these frequencies are close to those of the linearly unstable eigenmodes. The energy of the helical wave that results is time periodic, as the wave changes shape periodically with frequency $f_2 - f_1$, on observing it in a frame rotating at $\Omega + f_1$. A power spectrum of the mass flux or the energy therefore exhibits a single main peak at $f_2 - f_1$, plus its harmonics.

We are thus provided with a rough qualitative explanation of the $\alpha = 0.1$ results presented above (i.e. the existence of two independent unstable modes results in quasi-periodicity of the velocity field). However, owing to the higher degree of nonlinearity in that case, the secondary instability occurs at an axial Reynolds number of about 350, which is considerably less than the value 1200 which can be read off from the linear stability curves of Cotton & Salwen (1981).

The last set of computations we report were performed at fixed rotation and axial pressure gradient, whilst varying the pitch of the helices (i.e. the physical parameters are fixed, and the wavenumber of the flow disturbance is varied). With $R_z = 500$ and $\Omega = -0.5$, the basic flow is linearly unstable for $0.14 < \alpha < 1.2$. For α between 1.2 and 0.35 the flow consists of a steady rotating wave. As α is decreased from 0.35 to 0.30, a secondary Hopf bifurcation occurs leading to quasi-periodic flow, with simply periodic mass flux and energy (figure 9*a*). A new bifurcation has occurred by $\alpha = 0.275$, which is found to be a period doubling bifurcation (figure 9*b*). A cascade of period doublings appears as α is decreased further; by $\alpha = 0.265$ another two steps have occurred in the cascade (figure 9*c*). Although the data collected for the bifurcation points is sparse, comparison with the universal scaling for period-doubling bifurcations of Feigenbaum (1979) is in accordance with the theory.

At $\alpha = 0.25$ the flow appears to display non-periodic, or chaotic time dependence (figure 9*d*). This is diagnosed by computing the power spectrum of the energy or mass flux, which become broadband. Figure 10 displays some of the power spectra for these flows. Figure 10(*a*) corresponds to the behaviour of the mass flux after one period doubling, with one primary peak and its harmonics. Figures 10(*b*) and 10(*c*) are the spectra for the mass flux, and also a pointwise velocity measurement, in the chaotic regime. The velocity spectrum, like that for the mass flux, is broadband, but displays one primary peak, corresponding to the single convective fast timescale at which the vortex system rotates within the pipe. On viewing the actual vorticity dynamics for the non-periodic flow, one again sees similar phenomena as described in the energy-periodic regime above; however, the generation of a secondary positive vortex occurs irregularly in time. It is worth noting that for the physical parameters chosen, this behaviour occurs at wavenumbers whose growth rates are smaller than at $\alpha = 0.51$, where the maximum instability occurs according to linear theory, and where disturbances saturate to a steady rotating wave. The above set of computations was done with resolution $M = 15, N = 50$ (with a mild boundary layer stretching of $a_1 = 1, b_1 = 3$), which resolved the gradients of vorticity and produced a well-decaying energy spectrum.

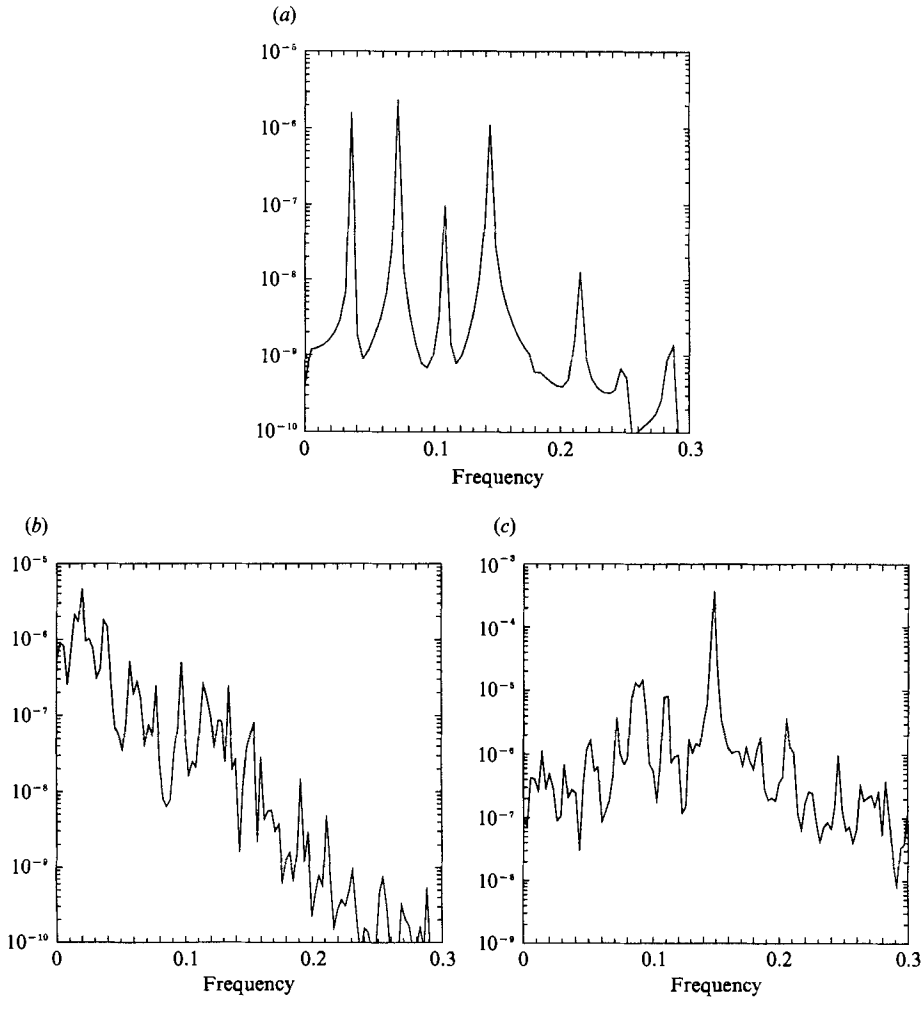

FIGURE 10. Power spectra, $R_z = 500$, $\Omega = -0.5$. (*a*) The mass flux when $\alpha = 0.275$ (period doubled). (*b*) The mass flux and (*c*) pointwise velocity, $\alpha = 0.25$ (non-periodic regime).

5. Discussion

We have presented the results of a direct simulation of the Navier–Stokes equations for rotating pipe Poiseuille flow, under the constraint that the solutions possess helical symmetry. The primary nonlinear steady rotating waves may become unstable through a Hopf bifurcation as the parameters R_z, R_Ω, or α are varied, leading to a quasi-periodic velocity field, but with simply periodic energy and mass flux. These secondary waves may undergo a futher series of bifurcations, which lead to chaotic temporal evolution. For the set of numerical computations we performed, the onset of chaos occurs through a period-doubling cascade. This bifurcation scenario has also been found in simulations of two-dimensional double-diffusive convection (Knobloch *et al.* 1986).

Our results have been confined to solutions of a single helical pitch, whereas in general the linear instability of a rotating pipe flow will occur for a continuum of helical waves. For instance, the computations we have performed for the linear and secondary instability of $\alpha = 1$ waves occurs when unstable helical waves at smaller α already exist (Cotton & Salwen 1981). The actual fully three-dimensional nonlinear

development of a rotating pipe flow is yet to be elucidated, although it is expected that large-scale instability will dominate in an uncontrolled experiment. The bifurcation results presented are of mathematical interest, however, and should be realizable in a controlled experiment.

A series of bifurcations leading to chaotic time dependence for streamwise periodic waves in two-dimensional plane Poiseuille flow has also been described by Jiménez (1990). In that geometry, however, the transition to temporal irregularity was through a series of Hopf bifurcations, with three-periodic flow being the precursor of chaos. As this and the period-doubling bifurcation scenario are ubiquitous in many nonlinear dynamical systems, we might also expect to find other routes to chaos in the spatially periodic helical wave system in different regimes of parameter space. In particular, it was demonstrated here that the flow became quasi-periodic owing to the simultaneous existence of two unstable eigenmodes of the system; thus complex oscillatory motion quite possibly arises as more modes interact with each other.

We now discuss the stability of Hagen–Poiseuille (non-rotating pipe) flow. Our simulations with $\Omega = 0$ and non-axisymmetric initial conditions suggest that stable helical waves cannot be supported by the flow, at least up to axial Reynolds numbers R_z of 4000 at order one axial wavenumbers α. These results are reported on further in Landman (1990). The analogous null result was reported by Patera & Orszag (1981), who sought axisymmetric equilibria in pipe flow up to $R_z = 4000$.

In agreement with the experimental results of Leite (1959), our simulations in a non-rotating pipe show that the non-axisymmetric components of an initial disturbance set up in fully developed pipe flow decay on a fast advective timescale, in comparison with the axisymmetric components which decay viscously. Thus, in accordance with the steady work of Toplosky & Akylas (1988), we are unable to corroborate the assertion of Smith & Bodonyi (1982) that steady helical waves exist at high R_z. Our results do not preclude the existence of such waves, however, as they may be temporally unstable, exist at higher R_z, or may be accessible from only a limited class of initial conditions.

Even so, it appears that the nonlinear instabilities observed experimentally at Reynolds numbers R_D of about 2000 are not a direct consequence of the existence of helically stable two-dimensional equilibria. This claim takes into account that the experimental Reynolds number R_D is based on mass flux, which would correspond to a pressure Reynolds number R_z fractionally higher than 2000, through the relationship of (15).

Nevertheless, in the light of the stability properties of rotating pipe flow, an explanation for the onset of instabilities in a non-rotating pipe may be furnished. This was suggested by Mackrodt (1976), who considered that in an experiment the residual angular momentum of the inlet flow would result in a rotating core of fluid in the pipe, separated from the walls by a boundary layer. In addition, Mackrodt pointed out that only minimal rotation is required in order to destabilize Poiseuille flow at high axial Reynolds number. This line of investigation is taken in Landman (1990), where the linear stability of a swirling Poiseuille flow satisfying the no-slip condition on a stationary pipe is studied. It is found that there is a minimum critical core swirl of $R_\Omega \approx -30$, which is fairly insensitive to the actual details of the swirl profile and holds for wavenumbers α up to $O(1)$ (the critical R_Ω for rotating pipe flow is -28).

Given that a residual core of fluid in solid-body rotation may be the appropriate mechanism for observed pipe-flow transition, our results on rotating helical waves might account for some of the temporal irregularity of such flows. In order to

quantify the effect of a swirling core on fully nonlinear Hagen–Poiseuille flow, we have modelled this flow by forcing the fluid equations so that the basic flow is one of core swirl superposed on Poiseuille flow (Landman 1990). We have observed that not only do instabilities exist similar to the solid-body swirl case studied here, but hysteresis (multiple stable states) is also possible. This type of behaviour is well known for the geometry of flow between rotating cylinders, in which helical waves can also be observed (Andereck, Liu & Swinney 1986).

The presence of core rotation remains a potentially attractive means of explaining the generation of equilibrium puffs associated with laminar–turbulent transition at axial Reynolds numbers R_D of approximately 2000 in Hagen–Poiseuille flow (Wygnanski & Champagne 1973). In fact, Bandyopadhyay (1986), in a striking experimental study of the structure of the puff at $R_D = 2200$, found a laminar helical motion within the plug of fluid in the upstream region of the puff.

An analogy to two-dimensional plane Poiseuille flow is therefore suggested. Computing the flow between parallel plates over a large streamwise domain, solitary wave modulations of the underlying nonlinear waves have been found (Jiménez, 1990), leading to two-dimensional localized travelling states. Although the basic periodic nonlinear waves are stable to superharmonic perturbations, long-wave instabilities are responsible for generating such solitary waves at Reynolds numbers where the undisturbed parabolic flow is also stable. Similarly, one can speculate that a train of helical waves might undergo a solitary wave modulation over a large domain. A fully three-dimensional instability of the helical motion might then generate the turbulence associated with the downstream portion of an equilibrium puff. Such a secondary three-dimensional instability of a helical wave equilibrium or quasi-equilibrium would thus be analogous to the secondary instabilities of two-dimensional equilibria in planar shear flows (Bayly, Orszag & Herbert 1988).

Without doubt one of the primary goals of any theory of laminar–turbulent transition in Hagen–Poiseuille flow must be the prediction of the critical Reynolds number R_D of close to 2000. Yet it appears that further investigation is warranted despite a century since Reynolds' discoveries.

Many thanks go to Steve Childress, Bill Henshaw, and Hank Strauss for their interest and invaluable help. I would like to acknowledge support from AFOSR 86-0352, DARPA F49620-87-C-0065, and an IBM Summer Research Fellowship. Computations were performed on the Cray X-MP at the San Diego Supercomputer Center.

REFERENCES

ANDERECK, C. D., LIU, S. S. & SWINNEY, H. L. 1986 Flow regimes in a circular Couette system with independent rotating cylinders. *J. Fluid Mech.* **164**, 155–83.

ADEBIYI, A. 1981 On the existence of steady helical vortex tubes of small cross-section. *Q. Jl Mech. Appl. Maths* **34**, 153–177.

BANDYOPADHYAY, P. R. 1986 Aspects of the equilibrium puff in transitional pipe flow. *J. Fluid Mech.* **163**, 439–458.

BAYLY, B. J., ORSZAG, S. A. & HERBERT, T. 1988 Instability mechanisms in shear-flow transition. *Ann. Rev. Fluid Mech.* **20**, 359–391.

CHESSHIRE, G. & HENSHAW, W. 1989 Composite overlapping meshes for the solution of PDE's. *J. Comput. Phys.* (Submitted).

CHILDRESS, S., LANDMAN, M. J. & STRAUSS, H. R. 1989 Steady motion with helical symmetry at large Reynolds number. In *Proc. IUTAM Symp. on Topological Fluid Mechanics* (ed. H. K. Moffatt & A. Tsinober), pp. 216–224. Cambridge University Press.

COTTON, F. W. & SALWEN, H. 1981 Linear stability of rotating Hagen-Poiseuille flow. *J. Fluid Mech.* **108**, 101–125.

FEIGENBAUM, M. J. 1979 The universal properties of nonlinear transformations. *J. Stat. Phys.* **21**, 669–706.

FOX, J. A., LESSEN, M. & BHAT, W. V. 1968 Experimental investigation of the stability of Hagen–Poiseuille flow. *Phys. Fluids* **11**, 1–4.

GARG, V. K. & ROULEAU, W. T. 1972 Linear spatial stability of pipe Poiseuille flow. *J. Fluid Mech.* **54**, 113–127.

JIMÉNEZ, J. 1990 Transition to turbulence in two-dimensional Poiseuille flow. *J. Fluid Mech.* **218**, 265–279.

KNOBLOCH, E., MOORE, D. R., TOOMRE, J. & WEISS, N. O. 1986 Transitions to chaos in two-dimensional double-diffusive convection. *J. Fluid Mech.* **166**, 409–448.

LANDMAN, M. J. 1990 On the generation of helical waves in pipe Poiseuille flow. *Phys. Fluids* A **2**, 738–747.

LANGFORD, W. F., TAGG, R., KOSTELICH, E. J., SWINNEY, H. L. & GOLUBITSKY, M. 1988 Primary instabilities and bicriticality in flow between counter-rotating cylinders. *Phys. Fluids* **31**, 776–785.

LEITE, R. J. 1959 An experimental investigation of the stability of Poiseuille flow. *J. Fluid Mech.* **5**, 81–96.

MACKRODT, P.-A. 1976 Stability of Hagen–Poiseuille flow with superimposed rigid rotation. *J. Fluid Mech.* **103**, 241–255.

MAHALOV, A. & LEIBOVICH, S. 1988 Amplitude expansion for viscous rotating pipe flow near a degenerate bifurcation point. *Bull. Am. Phys. Soc.* **33**, 2247.

MARCUS, P. S. 1981 Effects of truncation in modal representations of thermal convection. *J. Fluid Mech.* **103**, 241–255.

NAGIB, H. M., LAVAN, Z. & FEJER, A. A. 1971 Stability of pipe flow with superimposed solid body rotation. *Phys. Fluids* **14**, 766–768.

PARK, W., MONTICELLO, D. A. & WHITE, R. B. 1984 Reconnection rates of magnetic fields including the effects of viscosity. *Phys. Fluids* **27**, 137–149.

PATERA, A. T. & ORSZAG, S. A. 1981 Finite-amplitude stability of axisymmetric pipe flow. *J. Fluid Mech.* **112**, 467–474.

PEDLEY, T. J. 1969 On the instability of viscous flow in a rapidly rotating pipe. *J. Fluid Mech.* **35**, 97–115.

REYNOLDS, O. 1883 An experimental investigation of the circumstances which determine whether the motion of water shall be direct or sinuous, and of the law of resistance in parallel channels. *Phil. Trans. R. Soc. Lond.* **174**, 84–99.

RICHTMEYER, R. D. & MORTON, K. W. 1967 Difference methods for initial-value problems. J. Wiley & Sons.

SALWEN, H., COTTON, F. W. & GROSCH, C. E. 1980 Linear stability of Poiseuille flow in a circular pipe. *J. Fluid Mech.* **98**, 273–284.

SALWEN, H. & GROSCH, C. E. 1972 The stability of Poiseuille flow in a pipe of circular cross-section. *J. Fluid Mech.* **54**, 93–112.

SMITH, F. T. & BODONYI, R. J. 1982 Amplitude-dependent neutral modes in the Hagen–Poiseuille flow through a circular pipe. *Proc. R. Soc. Lond.* A **384**, 463–489.

TOPLOSKY, N. & AKYLAS, T. R. 1988 Nonlinear spiral waves in rotating pipe flow. *J. Fluid Mech.* **190**, 39–54.

WYGNANSKI, I. J. & CHAMPAGNE, F. H. 1973 On transition in a pipe. Part 1. The origin of puffs and slugs and the flow in a turbulent slug. *J. Fluid Mech.* **59**, 281–335.